Ed. **1998**, *37*, 1534 – 1537; i) Y. Kobuke, K. Morita, *Inorg. Chim. Acta* **1998**, *283*, 167 – 174.
[8] a) F. M. Menger, D. S. Davis, R. A. Persichetti, J.-J. Lee, *J. Am. Chem. Soc*. **1990**, *112*, 2451 – 2452; b) F. M. Menger, *Bol. Soc. Chil. Quim*. **1990**, *35*(1), 33 – 38.
[9] F. M. Menger, *Angew. Chem*. **1991**, *103*, 1104 – 1118; *Angew. Chem. Int. Ed. Engl*. **1991**, *30*, 1086 – 1100.
[10] K. Kano, J. H. Fendler, *Biochim. Biophys. Acta* **1978**, *509*, 289 – 299.
[11] At first, multilamellar vesicles from DPPC films were formed: R. R. C. New, *Liposomes: A Practical Approach*, IRL Press, Oxford, **1990**; from the multilamellar vesicles, unilamellar vesicles were prepared by the membrane extrusion method: R. C. MacDonald, R. I. MacDonald, B. P. M. Menco, K. Takeshita, N. K. Subbaro, L.-R. Hu, *Biochim. Biophys. Acta* **1991**, *1061*, 297 – 303.
[12] F. M. Menger, P. Aikens, *Angew. Chem*. **1992**, *104*, 919 – 921; *Angew. Chem. Int. Ed. Engl*. **1992**, *32*, 898 – 900.
[13] The relative activity of **1**, **2a** – **d**, and Gramicidin D was reliably reproduced in several experiments.
[14] P. Läuger, *Angew. Chem*. **1985**, *97*, 939 – 956; *Angew. Chem. Int. Ed. Engl*. **1985**, *24*, 905 – 922.
[15] H. Schindler, *Methods Enzymol*. **1989**, *171*, 225 – 253.
[16] On membranes formed from pure soybean lecithin without cholesterol, no channel activity was observed. The reason could be a higher mobility of the ion channel-forming compound in the cholesterol-containing membrane: P. L. Yeagle, *Biochem. Biophys. Acta* **1985**, *822*, 267 – 287. As with amphotericin B, a specific interaction of **2a**, **2c**, and **2d** with cholesterol is also possible: D. E. Mickus, D. G. Levitt, S. D. Rychnosvsky, *J. Am. Chem. Soc*. **1992**, *114*, 359 – 360.
[17] P. K. Mondal, B. K. Seal, A. S. Basu, *Z. Phys. Chem. (NF)* **1973**, *87*, 295 – 307.
[18] M. Mantal, P. Müller, *Proc. Natl. Acad. Sci. USA* **1972**, *69*, 3561 – 3566.

Aluminum Fluoride as a Storage Matrix for Atomic Hydrogen **

Gudrun Scholz,* Reinhard Stößer, Jan Alam Momand, Andrea Zehl, and Jeannette Klein

Atomic hydrogen H• can be stabilized for years in a suitably prepared AlF_3 powder matrix at temperatures $T \geq 300$ K (Figure 1). The hydrogen atoms are formed within the matrix by γ irradiation, essential OH groups in the crystallites serve as precursors for the H•. Thus, for the first time the stabilization of the reactive H• atoms has been achieved in a fluoride of the earth metals. A prerequisite for the formation and stabilization of the H• atoms is a special preparation of AlF_3 under quasi isobaric conditions,[1] in which, in chemically and thermally controlled reactions of α- and β-trihydrates of AlF_3,

[*] Dr. G. Scholz, Prof. Dr. R. Stößer, Dr. J. A. Momand, Dr. A. Zehl, Dr. J. Klein
Humboldt-Universität zu Berlin
Institut für Chemie
Hessische Strasse 1 – 2, 10115 Berlin (Germany)
Fax: (+49) 30-2093-7378
E-mail: gs@magneton.chemie.hu-berlin.de

[**] This work was supported by Deutsche Forschungsgemeinschaft and by the Fonds der Chemischen Industrie. We thank Dr. E. Janata (HMI Berlin), Dr. B. Ziemer, Dr. M. Päch and Dr. J. Bartoll (HU Berlin) for the assistance with the experimental work.

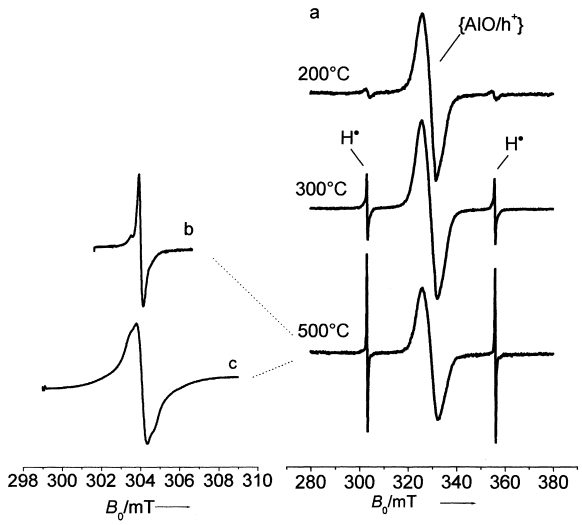

Figure 1. X-band ESR spectra (298 K) of trapped H• atoms: a) in AlF_3 powder samples of increasing crystallinity prepared from β-$AlF_3 \cdot 3H_2O$ under quasi isobaric conditions[1] at the temperatures given. b, c) Low-field signal of the trapped H• atoms in AlF_3, prepared by annealing of β-$AlF_3 \cdot 3H_2O$ at 500 °C ($P_{MW} = 2$ mW), measurement temperature 298 K (b), 4.2 K (c); the *y* axis scales are identical.

both the necessary cagelike structural elements and also the H• precursors are formed. Parallel to the long-term stability of the enclosed (trapped) H• atoms is the comparatively large values for the activation energies of their thermal decay. In addition it is noteworthy that the H• atoms fulfill the function of a spin probe in the solid-state samples. Compared to other paramagnetic dopants, such as transition metal ions,[2–5] the H• atoms are more suitable as a probe because their influence on the matrix is significantly lower. For example, both the spectral and spin dynamic ESR behavior and also the corresponding activation energies calculated from the thermal decay curves (Table 1) allow definitive conclusions to be drawn about the state of order in the matrix. These are in complete agreement with the findings from thermal analysis and X-ray diffraction. This form of direct relationship for trapped H• atoms has not been reported to date.

Table 1. Activation energies E_A and rate constants k for the thermally induced decrease in the H• signal in aluminum fluorides.

Annealing temperature [°C][a]	Annealing time [h]	k[b,c] [g mol^{-1} min^{-1}]	E_A [kJ mol^{-1}]
200	1	0.00576 (80) 0.02797 (110)	59.016
300	1	0.01148 (150) 0.08311 (200)	65.782
400	1	0.01084 (200) 0.06918 (250)	76.290
500	1	0.03668 (250) 0.11399 (280)	91.364
500	10	0.02624 (250) 0.08435 (280)	94.084

[a] The starting materials β-$AlF_3 \cdot 3H_2O$ were, in each case, annealed in a Q-crucible for 1 or 10 h under quasi isobaric conditions at the temperatures given. Following this they were subjected to γ irradiation. [b] Determined from the time dependent standard signal intensities. [c] The temperature [°C] for the decay reaction is given in each case in parentheses.

  1433-7851/00/3914-2516 $ 17.50+.50/0

Although there are numerous results demonstrating the chemical reactions and spectroscopy of atomic hydrogen at low temperature ($4.2 \leq T \leq 100$ K), only a few systems provide direct evidence for atomic hydrogen at $T \geq 298$ K.[6–23] Of these, all but one concern the fluoride and oxide compounds of alkali and alkaline earth metals and of silicon.[24] The discovery of the trapping of H$^{\bullet}$ in $Si_8O_{12}R_8$ compounds in the solid state[14, 18] as well as in solution[18] added a new dimension to the physics and chemistry of atomic hydrogen. The unexpected long-term stability, which can run into years in the solid state and from days to weeks in the solutions, permitted a detailed analysis of the chemical and physical properties of the stabilizing $Si_8O_{12}R_8$ structural units.[18] These cages are also suitable for the investigation of hyperfine coupling in muonium.[25]

However, when atomic hydrogen is trapped in aluminum fluoride powder (AlF_3/H$^{\bullet}$), its spectral and kinetic behaviors differ greatly. This is seen in a remarkable stability at room temperature, and can be readily identified in the products of thermal decomposition of the trihydrate after γ irradiation. For the α-$AlF_3 \cdot 3H_2O$ starting material this occurs in the temperature range $250\,^{\circ}C \leq T \leq 550\,^{\circ}C$ and for β-$AlF_3 \cdot 3H_2O$ in the range $200\,^{\circ}C \leq T \leq 650\,^{\circ}C$. Three typical X-band ESR spectra of the annealed and the γ-irradiated AlF_3 samples are shown in Figure 1a. In addition to the characteristic hyperfine structure of H$^{\bullet}$ ($^{1H}A = 50.9$ mT) is, centered between these two lines, the signal of another long-lived paramagnetic AlO/h$^+$ center[26]. The degree of order in the matrix is demonstrated by the line widths and shape of the hydrogen ESR signals. Thus the physical and chemical properties of the H$^{\bullet}$ atoms are clearly influenced by the matrix. With increasing temperature the line widths ΔB_{pp} of the H$^{\bullet}$-signals becomes noticeably smaller and the intensity of the signals increase relative to that of the AlO/h$^+$ center. Both paramagnetic centers benefit, to different extents because of their differing chemical natures, from the increasing idealization of the AlF_3 structure. There is a definite correlation between the line widths of the H$^{\bullet}$ signals, the particle size of the powder sample and, its amorphous content as determined by X-ray diffraction: With increasing particle size, decreasing amorphous content and therefore the increasing crystallinity of the samples, the line width decreases (Figure 2a, b). In the amorphous sections of the samples there is a statistical distribution of bond lengths and angles. This has a direct effect on the spin coupling parameters of the trapped H$^{\bullet}$ atoms. ESR experiments at different frequencies (S-, X-, Q-band; that is at 3.8, 9.5 and 34 GHz) indicate that these statistical effects are reflected in the distributions of the anisotropic hyperfine couplings. Of the chemical aspects, a modification of the s-electron density of the H atoms as a result of discriminating repulsive interactions in the cage substructure (see Figure 3d) appears more likely than a distribution of the *g*-components, which is dependent upon the comparatively high-lying excited states.[27] Spin-flip transitions[28] are spectroscopically less well defined than those of the $Si_8O_{12}R_8$ cage (see Figure 1b,[18]). Evidently the individual line widths in AlF_3 are considerably broader as a result of the interaction with the immediately adjacent ^{19}F nuclei. The spin relaxation (microwave saturation at $T \leq 10$ K) of the trapped H$^{\bullet}$ atoms is also very different to that of the $Si_8O_{12}R_8$ cage. In the spectrum of AlF_3/H$^{\bullet}$, saturation broadening occurs as a result of magnetic dipole–dipole interactions with the ^{19}F nuclei (Figure 1b, c). This broadening is accompanied by slight changes in the signal amplitudes.

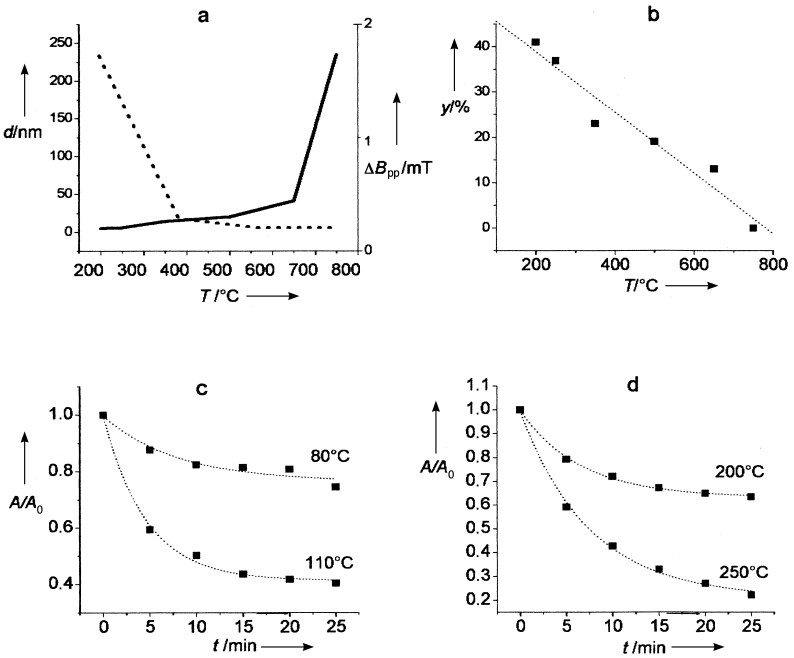

Figure 2. Annealing experiments with β-$AlF_3 \cdot 3H_2O$: a) influence of temperature on the particle size *d* of the product and on the line width ΔB_{pp} (••••) of the low-field signal of the trapped H$^{\bullet}$ atoms. b) Standardized amorphous content *y* in the annealed β-$AlF_3 \cdot 3H_2O$ samples as a function of the annealing temperature. c) Course of the decay of H$^{\bullet}$ atoms in AlF_3 against time, at 80 and 110 °C. Measurement temperature given as a function of the standard amplitude A/A_0; annealing temperature 200 °C. d) Course of the decay of H$^{\bullet}$ atoms in AlF_3 against time, at 200 and 250 °C. Measurement temperature given as a function of the standard amplitude A/A_0; annealing temperature 400 °C.

The AlF_3 matrix, because of the Pauli repulsion (see also CaF_2/H$^{\bullet}$[7, 17]), is clearly able to stabilize the H$^{\bullet}$ atoms over a wide temperature range.[29] Figures 3a–d show sections of the structures of CaF_2 and AlF_3 and of the local cages capable of incorporating H$^{\bullet}$ atoms. The time-dependent decrease of the H$^{\bullet}$ signals in AlF_3 (Figure 2c, d) demonstrate the direct dependence of the kinetic parameters of the trapped H$^{\bullet}$ atoms on the degree of order within the matrix. While in a sample annealed at 200 °C (amorphous content 41%) H$^{\bullet}$ atoms and their thermal decay can not be observed above 110 °C, in a sample annealed at 400 °C (amorphous content 20%) the H$^{\bullet}$ atoms are significantly more stable and the thermal decay can be monitored up to 250 °C (Figure 2c, d). For the macroscopic features this result is in agreement with the general observation that amorphous and structurally imperfect systems show greater chemical reactivity. An additional consideration here is that at higher temperatures, stabilized H$^{\bullet}$ atoms require a *symmetrical* environment, which, because of the repulsive

  1433-7851/00/3914-2517 $ 17.50+.50/0

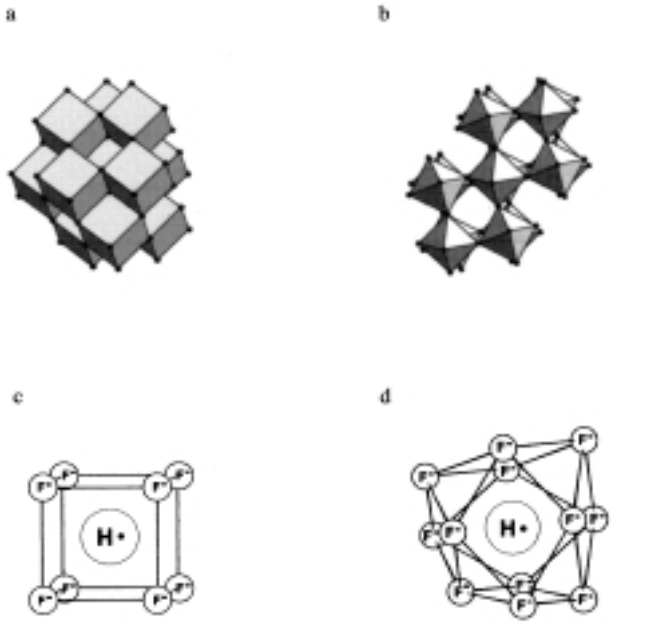

Figure 3. Sections of the structures of a) CaF_2 (space group $Fm\bar{3}m$) and b) α-AlF_3 (space group $R\bar{3}c$); local structure of the cages, formed by F atoms, which are suitable for taking up H• (from consideration of the van der Waals radius of H•): c) in CaF_2: $R_{F-F} = 2.709$ (neighboring), 4.709 Å (diagonal); d) in α-AlF_3: $R_{F-F} = 2.541$, 3.065, 4.105, 5.032 Å.

interactions, prevents the H• atoms from entering into chemical reactions or from leaving the cage. The experimental thermal decay curves (ESR intensity–time profiles, Figure 2c, d) can only be sensibly interpreted in terms of a second-order rate law leading to the rate constants and activation energies listed in Table 1. It is clear that the matrices with the greatest amorphous content give the lowest activation energies. Thus, in contrast to the molecular case[18] these experimental results support the idea that remote structural elements are involved in the stabilization of the H•. The necessary mobility of the potential reaction partners for the H• decay can be assumed.

The presence of precursors localized within the volume of the crystallites have been shown to be favorable for the long-term trapping of H• in AlF_3. Suitable prerequisites are created by the dehydration of AlF_3 hydrates under quasi isobaric conditions.[1] Treatment of the surfaces of (dehydrated) AlF_3 samples with D_2O gave the typical signals for trapped D• atoms, but only with 3–5% of the intensity of the simultaneously trapped H• atoms. Furthermore, it could be demonstrated that after γ irradiation at 300 K pure crystalline samples of CaF_2 and Na_3AlF_6 showed no trace of H•. In sharp contrast the corresponding OH contaminated powders gave, under the same conditions, intense ESR signals for trapped H• atoms. Generally the yield of H• at room temperature sinks considerably as the number of mobile H_2O molecules, OH groups, or H-bridging networks increases. H• atoms could not be trapped in the α- and β-$AlF_3 \cdot 3H_2O$ samples at $T \geq 300$ K. However, at lower temperatures ($T \leq 100$ K) even in these systems H• atoms could be stabilized in easily detectable concentrations.[26] Further support comes from the results obtained with the hydrates of calcium sulfate: At room temperature H• could only be trapped in the semi-hydrate ($CaSO_4 \cdot 0.5H_2O$).[8, 11] Similar results have so far not been reported for the dihydate.

In general the concentration of the hydrogen atoms generated and stabilized is dependent upon the nature and concentration of the transition metal ions incorporated. In AlF_3, for example, it can be shown that at Fe^{3+} concentrations above 0.1 mol% the rapid recombination of radiation defects is more effective and thus increasingly hinders the trapping of reactive species.

Experimental Section

The investigative methods used were multifrequency ESR spectroscopy (S-, X-, Q-band) in conjunction with thermal analysis, targeted chemical experiments and X-ray diffraction. ESR is the method of choice for the unambiguous detection of trapped H• atoms. In the X-band the temperature range from $4.2 \leq T \leq 600$ K can be used for the characterization of H•; that is, an observation window of over 500 degrees is available. ESR spectroscopy exploits the specific hyperfine patterns (Figure 1) to provide a simple and direct method to detect H• atoms. All ESR investigations were carried out in the μW region, or significantly below microwave saturation (max. 2 mW). A ^{60}Co source was used for the γ irradiation and an average dose of 100 kGy employed. The samples were thermally prepared in an oven by using a labyrinth Pt crucible (Q-crucible).[1] Each of the starting materials (α- and β-$AlF_3 \cdot 3H_2O$) were annealed for 1 h at temperatures between 50 and 800 °C. The results obtained were completely reproducible. Different charges of AlF_3 obtained from different preparations were employed. After appropriate thermal treatment both α- and β-$AlF_3 \cdot 3H_2O$ led to products that can, after γ irradiation, capture H• atoms. Differences occur in terms of the yields and the chemical and spin dynamic behavior of the trapped H• atoms.

Received: December 22, 1999 [Z14446]

[1] G. Scholz, R. Stösser, S. Sebastian, E. Kemnitz, J. Bartoll, *J. Phys. Chem. Sol.* **1999**, *60*, 153–162.
[2] G. Scholz, *J. Solid State Chem.* **1998**, *139*, 27–36.
[3] G. Scholz, R. Stösser, T. Grande, S. Aasland, *Ber. Bunsen-Ges. Phys. Chem.* **1997**, *101*, 1291–1296.
[4] R. Stösser, G. Scholz, *Appl. Magn. Res.* **1997**, *12*, 167–181.
[5] R. Stösser, G. Scholz, *Appl. Magn. Res.* **1998**, *15*, 449–468.
[6] E. Duval, J. Serughetti, R. Louat, *Solid State Comm.* **1970**, *8*, 1155–1158.
[7] S. L. Sligar, H. Blum, *Phys. Rev. B* **1971**, *3*, 3587–3592.
[8] H. Kon, *J. Chem. Phys.* **1964**, *41*, 573–574.
[9] R. G. Bessent, W. Hayes, J. W. Hodby, P. H. S. Smith, *Proc. R. Soc. London A* **1969**, *309*, 69–90.
[10] B. Welber, *Phys. Rev. A* **1964**, *136*, 1408–1412.
[11] A. M. Belongov, A. G. Grammakov, A. S. Serdjuk, S. A. Suppé, *Proc. Colloq. AMPERE* **1970**, *16*, 943.
[12] N. Papp, K. P. Lee, *J. Magn. Reson.* **1975**, *19*, 245–249.
[13] L. E. Iton, J. Turkevich, *J. Phys. Chem.* **1978**, *82*, 200–214.
[14] R. Sasamori, Y. Okane, T. Isobe, Y. Matsuda, *Science* **1994**, *265*, 1691–1693.
[15] K. Ogoh, S. Takaki, C. Yamanaka, M. Ikeya, E. Ito, *J. Phys. Soc. Jpn.* **1996**, *65*, 844–847.
[16] R. A. B. Devine, K. Hübner, *Phys. Rev. B* **1989**, *40*, 7281–7283.
[17] J. L. Hall, R. T. Schumacher, *Phys. Rev.* **1962**, *127*, 1892–1912.
[18] M. Päch, R. Stößer, *J. Phys. Chem. A* **1997**, *101*, 8360–8365.
[19] F. Hill, G. Lehmann, *Z. Naturforsch. A* **1978**, *33*, 1484–1486.
[20] J. M. Baker, A. Cox, A. J. O'Connell, R. C. C. Ward, *J. Phys. Condens. Matter* **1991**, *3*, 6189–6193.
[21] Y. Ueda, Y. Kazumata, M. Nishi, *Jpn. J. Appl. Phys.* **1977**, *16*, 1743–1745.
[22] A. V. Egranov, V. V. Otroshok, B. P. Chernyago, *Phys. Status Solidi B* **1991**, *167*, 451–458.
[23] A. V. Egranov, *Phys. Status Solidi B* **1993**, *179*, 323–327.

  1433-7851/00/3914-2518 $ 17.50+.50/0

[24] LiF:OH^-,[6] CaF_2,[7, 13, 17] $CaSO_4 \cdot 0.5\,H_2O$,[8, 11] BaF_2,[9, 10] $BaSO_4$,[11] SiO_2 surface,[12] $Si_8O_{12}R_8$-cage,[14, 18] SiO_2 high-pressure modifications,[15, 16] $NaAl_3(OH)_4(PO_4)_2$,[19] Li_2O,[20, 21] LiF:H^-, Mg^{2+}.[22, 23]
[25] H. Dilger, E. Roduner, R. Scheuermann, J. Major, M. Schefzik, R. Stößer, M. Päch, D. G. Fleming, *Phys. Condens. Matter* **1999**, in press.
[26] R. Stößer, J. Bartoll, L. Schirrmeister, R. Ernst, R. Lück, *Appl. Radiat. Isot.* **1996**, *47*, 1489 – 1496.
[27] P. J. Bruna, G. H. Lushington, F. Grein, *Chem. Phys. Lett.* **1996**, *258*, 427 – 430.
[28] Detectable as satellites on the hyperfine lines of the H· atoms.[18]
[29] F. J. Adrian, *J. Chem. Phys.* **1960**, *32*, 972 – 981.

Intermediate-Range Order in Amorphous Nitridic Ceramics: Lessons from Modern Solid-State NMR Spectroscopy**

Leo van Wüllen, Utz Müller, and Martin Jansen*

Structural characterization and theoretical modeling of crystalline solids are only possible because of their translational symmetry. Once the translatorial periodicity is lost, as in quasicrystals and amorphous networks, the structural characterization of these solids, a prerequisite for a profound understanding of the physical and chemical properties, becomes a rather tedious task. This lack of routine methods for the structural characterization of amorphous solids is the reason for an only limited understanding of scientifically and industrially important systems.

Amorphous ceramics in the system boron, silicon, carbon, and nitrogen have gained considerable importance as high-performance ceramic materials due to their exceptional stability at high temperatures and their resistance to oxidation.[1] Among these ceramics, those obtained by ammonolysis, polycondensation, and subsequent pyrolysis of single-source precursors have been ascribed superior characteristics with respect to resistance to crystallization and homogeneity.[2] The ternary ceramic $Si_3B_3N_7$ and the quaternary ceramic $SiBN_3C$ are the best studied so far with respect to structural details.[3] A structural characterization of these amorphous systems can only be successful if a combination of characterization methods is used, each predominantly probing the short-, intermediate-, or long-range order. Modern solid-state NMR spectroscopy is emerging as one of the most powerful tools in this field. The short-range order in a range of 1 – 2 Å was successfully elucidated by magic angle spinning (MAS) NMR methods. These studies found trigonally planar BN_3 and tetrahedral SiN_4 polyhedra as the basic building blocks constituting the network. Transmission electron spectroscopy studies revealed[4] that the amorphous network in these ceramics is homogeneous with respect to an elemental distribution on a subnanometer scale. To date, the intermediate-range order, corresponding to a length scale of 2 – 5 Å has not yet been accessible. This gap is closed with the present study, by utilizing modern double resonance solid-state NMR methods. As a first characterization of the ceramic $Si_3B_3N_7$ the solid-state NMR single-pulse MAS solid-state spectra were recorded. The signals with isotropic chemical shifts of $\delta = -45.2$ (^{29}Si MAS-NMR) and 30.4 (^{11}B MAS NMR) indicate a local environment consisting of BN_3 and SiN_4 units, as confirmed by a comparison to the spectra of the binary model compounds h-BN and α-Si_3N_4 and β-Si_3N_4, respectively.[5]

The intermediate-range order, originating in the interconnection of the polyhedra to give the resulting amorphous network, was traced by employing rotational echo double resonance (REDOR) NMR spectroscopy.[6] In this approach, the heteronuclear dipolar interaction between two nuclear species I and S, averaged out under the conditions of the MAS experiment, is reintroduced by rotor-synchronized 180° dephasing pulses for the S spins. The signal of the first nuclear species I is detected by using a rotor-synchronized solid-state spin-echo pulse sequence. The 180° pulses for the second nuclear species (S) produce a sign shift of the heteronuclear dipolar Hamiltonian, resulting in a decreased echo amplitude *S*. A conventional spin echo experiment for the I spins provides the maximum echo amplitude S_0. Simulations of the resulting dipolar evolution curve, obtained as a plot of the normalized difference $\Delta S/S_0$ as a function of the dipolar evolution time—the product of the number of rotor cycles N and the rotor period T_R—then allows a direct determination of the ^{11}B-^{29}Si internuclear distance in the case of an isolated two-spin system. Comparing the two principally feasible experiments ^{29}Si{^{11}B}-REDOR and ^{11}B{^{29}Si}-REDOR NMR the first would be the natural choice because of the natural abundance of the two isotopes ^{29}Si (4.7 %) and ^{11}B (80.4 %). The quadrupolar nature of the isotope ^{11}B (nuclear spin = 3/2) as the dephasing nucleus however severely complicates data analysis.[7] Therefore we decided to perform the second variant, ^{11}B{^{29}Si} REDOR. This makes the use of a 100 % ^{29}Si isotopically enriched sample of $Si_3B_3N_7$ vital, since in a ^{11}B-{^{29}Si}-REDOR experiment on a sample containing ^{29}Si in natural abundance only approximately 5 % of the actual B-Si dipolar couplings would be detected.

Figure 1 contains a compilation of ^{11}B-{^{29}Si}-REDOR spectra for dipolar evolution times of 0.4, 1.2, and 2 ms together with the resulting REDOR curve. The lineshape of the ^{11}B resonance is dominated by the second-order quadrupolar interaction, which is not completely averaged out even under the conditions of fast MAS. Line shape analysis yields a quadrupolar coupling constant of 2.9 MHz and an asymmetry parameter η of 0.1. Figure 1 a shows the results of ^{11}B-spin-echo experiments, Figure 1 b the ^{11}B{^{29}Si}-REDOR spectra. The difference of the two experiments is plotted in Figure 1 c. An increase of the difference intensity $S - S_0$ with increasing dipolar evolution time becomes obvious.

[*] Prof. Dr. M. Jansen, Dr. L. van Wüllen
Max-Planck-Institut für Festkörperforschung
Heisenbergstrasse 1, 70569 Stuttgart (Germany)
Fax: (+49) 711-689-1502
E-mail: martin@jansen.mpi-stuttgart.mpg.de
Dipl.-Chem. U. Müller
Institut für Anorganische Chemie
Rheinische Friedrichs-Wilhelms-Universität Bonn
Gerhard-Domagk-Strasse 1, 53121 Bonn (Germany)

[**] This work was supported by the Deutsche Forschungsgemeinschaft (SFB 408).

  1433-7851/00/3914-2519 $ 17.50+.50/0